Stage-dependent changes of β2-adrenergic receptor signaling in right ventricular remodeling in monocrotaline-induced pulmonary arterial hypertension

FENGJIAO SUN[1*], ZHIQIANG LU[2*], YIDAN ZHANG[1], SHIHAN GENG[1], MENGXI XU[1], LIMAN XU[1], YINGYING HUANG[1], PENGWEI ZHUANG[1,3] and YANJUN ZHANG[1,3]

[1]Tianjin State Key Laboratory of Modern Chinese Medicine, Tianjin University of Traditional Chinese Medicine, Tianjin 300193; [2]Department of Pharmacology, School of Pharmaceutical Science and Technology, Tianjin University, Tianjin 300072; [3]Department of Pharmacology, Chinese Materia Medica College, Tianjin University of Traditional Chinese Medicine, Tianjin 300193, P.R. China

Received June 20, 2017; Accepted January 10, 2018

DOI: 10.3892/ijmm.2018.3449

Abstract. Right ventricular (RV) remodeling coupled with extensive apoptosis in response to unrestrained biomechanical stress may lead to RV failure (RVF), which is the immediate cause of death in the majority of patients with pulmonary arterial hypertension (PAH). Overexpression of β_2-adrenergic receptor (β_2-AR) signaling has been reported to induce myocardiotoxicity in patients with left heart failure. However, the role of β_2-AR signaling in the pathophysiology of PAH development has remained elusive. To address this issue, the present study investigated the changes in cardiopulmonary function and structure, as well as the expression of regulators of fibrosis and apoptosis in RVF following monocrotaline (MCT; 60 mg/kg, i.p.)-induced PAH in rats. Cardiopulmonary function and structure, remodeling and apoptosis, as well as G protein-coupled receptor (GPCR) and β_2-AR signaling, were documented over a period of 6 weeks. In the early stages, elevated pulmonary arterial pressure, pulmonary lesions, RV hypertrophy, evidence of left ventricular (LV) hyperfunction and accelerated heart rate were observed in animals with MCT-induced PAH. The levels of angiotensin II receptor type 1b (Agtr1b), Agtr2 and Agt were markedly upregulated and the expression of β_2-AR phospho-Ser(355,356) steadily decreased in the right heart. As the disease progressed, LV dysfunction was observed, as evidenced by decreased LV systolic pressure and increased LV end-diastolic pressure, which was accompanied by a sustained increase in circulating brain natriuretic peptide levels. Of note, increased levels of cardiomyocyte apoptosis and concomitant RV remodeling, including hypertrophy, dilatation, inflammation and fibrosis, were observed, despite the enhanced RV contractility. Furthermore, alterations in GPCR signaling and activation in β_2-AR-G_s-protein kinase A/Ca^{2+}/calmodulin-dependent kinase II signaling were observed in the late stages of PAH. These results suggested that treatment with MCT results in adaptive and maladaptive RV remodeling and apoptosis during the progression of PAH, which is accompanied by distinct changes in the β_2-AR signaling. Therefore, these results enable researchers to better understand of pathophysiology of MCT-induced PAH, as well as to determine the effects of novel therapies.

Correspondence to: Professor Yanjun Zhang or Professor Pengwei Zhuang, Department of Pharmacology, Chinese Materia Medica College, Tianjin University of Traditional Chinese Medicine, 312 Anshanxi Road, Nankai, Tianjin 300193, P.R. China
E-mail: zyjsunye@163.com
E-mail: zhuangpengwei@163.com

*Contributed equally

Key words: β2-adrenergic receptor signaling, right ventricular remodeling, apoptosis, pulmonary arterial hypertension, monocrotaline

Introduction

Pulmonary arterial hypertension (PAH) comprises a group of disorders that involve pulmonary vasoconstriction and vascular remodeling, as well as right ventricular (RV) hypertrophy (1,2). The response of the RV to the increased afterload, including electrical, mechanical and structural changes, may ultimately induce left ventricular (LV) atrophic remodeling and dysfunction (3,4). RV failure (RVF) in particular is the immediate cause of death in the majority of PAH patients (1,2). Clinically updated techniques and approved PAH-specific therapeutic agents have been effectively applied to identify RV dysfunction and improved the quality of life of the respective patients (5,6). However, PAH is associated with a poor outcome with an estimated 5-year survival rate of <60% (7).

The key role of RV remodeling in PAH has received increasing attention, as larger volumes, pathological hypertrophy, diffuse inflammatory infiltration and interstitial fibrosis adversely were reported to affect the ejection fraction and ultimately lead to ventricular failure (1,2,8-12).

Myocardial apoptosis, a highly regulated process of cell death, has also been reported to occur in a rat model of monocrotaline (MCT)-induced PAH and may have an important role in cardiac remodeling after PAH (10,11). Therefore, remodeling as well as apoptosis have key roles in the pathogenesis of RV maladaptation and failure.

β-adrenergic receptor (β-AR) signaling is a primary event in the regulation of myocardial contractility under normal physiological conditions, whereas its sustained activation also contributes to myocardial dysfunction during the progression of heart failure (HF). It has been confirmed that overexpression of human β_1-AR leads to early hypertrophy and interstitial fibrosis, followed by marked cardiac dysfunction in transgenic mice (13). Several studies reported that Ca^{2+}/calmodulin-dependent kinase II (CaMKII) mediates β-AR-induced myocyte death through either a protein kinase A (PKA)-dependent or a PKA-independent process (14,15). Of note, β_1-AR activation enhances cardiomyocyte apoptosis, whereas β_2-AR exerts anti-apoptotic effects on the heart. This crucial difference between the two receptor subtypes is associated with the signaling of β_2-AR through the inhibitory G protein (G_i), which improves cardiac function and decreases apoptosis (16,17). In contrast to the current dogma, recent studies demonstrated that β_2-AR signaling may also have cardiotoxic effects (17-21). In certain types of HF, β_2-AR signaling may lose its normally cardioprotective properties and change to β_1-AR-like global signaling, thus contributing to the HF phenotype (22). In addition, accumulating evidence demonstrated that β_2-AR activation increases the risk of sudden cardiac death in HF patients, and that non-selective β-AR blockade provides a greater survival benefit compared with selective β_1-AR blockade in chronic HF patients (23,24). Thus, a state of toxic and protective effects coexists with respect to the β_2-AR status in HF. However, the role of β_2-AR signaling in the progression of PAH has not been fully elucidated.

To investigate this issue, the present study used a rat model of MCT-induced PAH, since it is an informative animal model for identifying the progression of cardiopulmonary alterations associated with a profound remodeling of the heart with RV hypertrophy and dysfunction (25-28). In the present study, the time-course of the alterations of cardiopulmonary function and structure was investigated during the progression of PAH. In addition, the potential roles of G protein-coupled receptor (GPCR) signaling and further β_2-AR signaling in the progression of the pathophysiology of MCT-induced PAH were determined in a stage-dependent manner.

Methods

MCT-induced PAH. The present study conformed to the Guide for the Care and Use of Laboratory Animals published by the National Institutes of Health (NIH) and all of the procedures were approved by the Animal Ethics Committee of Tianjin University of Traditional Chinese Medicine (Tianjin, China; no. TCM-LAEC2015034). A total of 160 Male Wistar rats (age, 7 weeks; weight, 180-200 g; certificate no. SCXK 2012-0001) were obtained from Beijing Vital River Laboratory Animal Technology Co., Ltd. (Beijing, China). The rats were maintained at a room temperature of 22±2˚C and humidity of 50±5%, with a 12 h light/dark cycle. Food and water were available ad libitum. The PAH rat model was induced by a single intraperitoneal injection of MCT (60 mg/kg body weight; GuangRun Bio Technology, Co., Ltd., Nanjing, China) as described in a previous study by our group (29). Saline-injected rats served as the control (CON) group. At week 0 (prior to the MCT injection), and at weeks 1-6, cardiopulmonary function and pathology, as well as the molecular mechanisms underlying RV remodeling and apoptosis were compared between the CON and MCT-treated rats (n=10/group) at a total of seven sequential time-points.

Lung respiratory function. Pulmonary respiratory function, including respiratory frequency (RF), tidal volume (TV) and minute volume (MV), were measured using whole-body barometric plethysmography (WBP PLT-UNR-RT-2; EMKA Technologies, Paris, France). The rats were placed in a whole-body plethysmograph and were allowed to acclimatize for at least 10 min prior to analysis. The box pressure wave was recorded via a transducer and computer system (iOX2 software; version 2.5; EMKA Technologies) and the measurements were recorded.

Pulmonary artery pressure, RV and LV haemodynamics. Baseline hemodynamic data were obtained during the routine pulmonary artery, right and left heart catheterization, as previously described (30). In brief, the rats were anesthetized with pentobarbital sodium (50 mg/kg) and a cervical midline skin incision was performed. The right carotid artery was cannulated with a polyethylene catheter [PE-50; 0.58 mm inner diameter (ID); 0.99 mm outer diameter (OD); American Health & Medical Supply International Corp. Co., Ltd., Scarsdale, NY, USA]. LV systolic pressure (LVSP), LV end-diastolic pressure (LVEDP) and heart rate (HR) were measured via this catheter, which was advanced into the LV cavity, and the parameters were recorded with a PowerLab System (ML870 PowerLab; AD Instruments Pty Ltd., Sydney, Australia) to obtain the maximum rates of LV pressure increase and decrease as a measure of systolic and diastolic function, respectively (LV $+dP/dt_{max}$ and $-dP/dt_{min}$). The right jugular vein was cannulated with a micro-urethane catheter (BB520-40, 0.635 mm ID, 1.02 mm OD; American Health & Medical Supply International Corp. Co., Ltd.) and, after recording the RV hemodynamic data [RV systolic pressure (RVSP), RV end-diastolic pressure (RVEDP), and maximal rate of RV pressure increase and decrease (RV $+dP/dt_{max}$ and $-dP/dt_{min}$, respectively)], the measuring catheter was advanced across the pulmonary valve into the pulmonary artery to measure the pulmonary artery systolic pressure (PASP) and pulmonary arterial diastolic pressure (PADP). All these data were entered into a computer using PowerLab 8 channel physiological recorder and analyzed using LabChart 7.3.7 software (AD Instruments Pty Ltd., Sydney, Australia). Following hemodynamic measurements, the animals were euthanized for further processing.

Serum brain natriuretic peptide (BNP) level assessment. Blood samples were collected and centrifuged at 1,000 x g at 4˚C for 15 min to separate the supernatant. Serum BNP was detected with an ELISA kit (cat. no. CSB-E07972r; Cusabio Biotech Co., Ltd., Wuhan, China) according to the manufacturer's protocols.

Gross evaluation. The lungs and heart were rapidly dissected and weighed. The lung index was assessed as follows: Lung index = [total lung wet weight (g)/body weight (g)] x100. The heart was divided into RV and LV including the intraventricular septum (defined as LVS) to calculate the RV/LVS weight ratio, which resembled the RV hypertrophy index (RVHI). The RV wall was snap-frozen and stored at -80˚C for further analysis.

Histological analysis. Heart and lung tissues were fixed with 10% formaldehyde, embedded in paraffin, sectioned at 3.5-4 μm intervals, stained with hematoxylin and eosin staining (H&E, hematoxylin for 10 min, followed by counterstaining with eosin for 4 min at room temperature) and visualized under a Leica DM4000B LED light microscope equipped with a Leica DFC450C camera (Leica Microsystems, Wetzlar, Germany). Interstitial fibrosis of the RV was determined by using a Masson's trichrome-staining kit (cat. no. G1340; Beijing Solarbio Science & Technology Co., Ltd., Beijing, China) according to the manufacturer's protocol. Briefly, deparaffinization and rehydration were accomplished as follows: immersion in xylene, twice (5 min each); 100% ethanol, twice (5 min each); immersion in 95% ethanol, twice (5 min each); distilled water (5 min). These sections were stained with hematoxylin-iodineferric chloride solution (1:1) for 10 min at room temperature, differentiated in hydrochloride-alcohol solution for 6 sec and then quickly rinsed under running tap water (15 min). Sections were stained in ponceau staining solution (8 min, room temperature) and then quickly rinsed in phosphomolybdic acid solution (1%, room temperature). The sections were stained with aniline blue solution and followed by dehydration through a series of alcohols (95%, three times; 100%, twice) to xylene (3 times) and then coverslipped. The collagen fibers appeared blue. Micrographs were captured from each sample at x400 magnification and quantified using ImageJ software (version 1.42q; NIH, Bethesda, MD, USA).

Terminal deoxynucleotidyl transferase (TdT) deoxyuridine triphosphate nick end labeling (TUNEL) assay. The TUNEL assay was performed using the *In Situ* Cell Death Detection kit (POD; cat. no. 11684817910; Roche Applied Science, Mannheim, Germany), according to the manufacturer's instructions. Following deparaffinization and rehydration, the sections were treated with 3% H_2O_2 in methanol for 10 min, and then incubated with proteinase K (20 μg/ml in 10 mM Tris/HCl, pH 7.4) for 30 min at 37˚C. The slides were immersed in TUNEL reaction mixture for 60 min at 37˚C in a humidified atmosphere in the dark. A converter peroxidase was added, followed by incubation of the slides for 30 min. The reaction was developed with diaminobenzidine substrate (brown) and counterstained with hematoxylin (blue). Negative (omission of TdT) and positive controls (treatment of the sections with DNase I for 10 min at room temperature prior to labeling procedures) were prepared for contrast. TUNEL-positive cells were defined as cells with clear brown or brown-blue nuclear labeling. To assess the TUNEL index of the RV, 10 micrographs per tissue section were randomly selected at a magnification of x400. The TUNEL index (%) was calculated as the ratio of the number of TUNEL-positive cells divided by the total number of cells.

RNA isolation and reverse transcription-quantitative polymerase chain reaction (RT-qPCR) GPCR arrays. The expression levels of 84 GPCR-associated genes were quantified using a G-Protein-Coupled Receptor Signaling Pathway Finder™ PCR Array from SA Biosciences (Qiagen, Hilden, Germany) at weeks 1, 3, 5 and 6 (corresponding to groups 1, 3, 5 and 6). Total RNA from RVs was isolated using the Qiagen RNA extraction kits (cat. no. 74704; Qiagen) in accordance with the manufacturer's protocols. Complementary (c)DNA was synthesized from 1 μg RNA using the SABiosciences RT^2 First Strand kit (cat. no. 330401; Qiagen). Of the 84 genes analyzed by the cDNA array, 95% were amplified with Ct values of <35 cycles by qPCR and were considered to be suitable for relative expression analysis. RT-qPCR was performed by using the RT^2 Profiler PCR Array Rat GPCR kit (cat. no. 330231; Qiagen). The reaction conditions comprised 1 cycle of initiation at 95˚C for 10 min, followed by 40 cycles at 95˚C for 15 sec and 60˚C for 1 min using the ABI 7500 Fast Real-Time PCR System (Applied Biosystems; Thermo Fisher Scientific, Inc., Waltham, MA, USA). Each 96-well plate included primers for five housekeeping genes, as well as positive and negative controls. The ΔCt method was used for PCR array data analysis (31,32). Only expression values with a difference of >2- or <0.5-fold with respect to the controls were considered statistically significant. Three repeated tests were performed for each set of measurements and the resulting data were averaged.

Protein analysis of β-AR signaling. Standard western blot analysis was performed using RV lysates, as previously described (33). The proteins were probed with the following primary antibodies: Rabbit anti-tubulin (1:500 dilution; cat. no. SC-91C4; Santa Cruz Biotechnology, Inc., Danvers, MA, USA), rabbit anti-β_1-AR (1:1,000 dilution; cat. no. ab3442) rabbit anti-β_2-AR (1:1,000 dilution; cat. no. ab137494) and rabbit anti-G protein-coupled receptor kinase 2 (GRK2; 1:500 dilution; cat. no. ab32558; all from Abcam, Cambridge, MA, USA), rabbit anti-phospho (p)-β_2-AR (pSer346; 1:1,000 dilution; cat. no. SAB4504272) and rabbit anti-p-β_2-AR [pSer(355,356); 1:500 dilution; cat. no. SAB4504074; both from Sigma-Aldrich; Merck KGaA, Darmstadt, Germany], rabbit anti-PKA (1:1,000 dilution; cat. no. 06-903; EMD Millipore, Billerica, MA, USA) and rabbit anti-CaMKII (1:1,000 dilution; cat. no. 3362; Cell Signaling Technologies, Inc., Danvers, MA, USA). Horseradish peroxidase-conjugated goat anti-rabbit immunoglobulin G (1:3,000 dilution; cat. no. ZB-2301; Zhongshan Goldenbridge Bio, Beijing, China) was used as a secondary antibody. Enhanced chemiluminescence (WBKLS0500; Merck KGaA) was visualized using a Vilber Fusion FX7 RT-ECL scanner (Vilber Lourmat, Marne-la-Vallée, France). Band signals were quantified by densitometry with Bio1D software (version 15.06a; Vilber Lourmat). The protein expression data of β_1-AR, β_2-AR, PKA, GRK2 and CaMKII were normalized to tubulin, whereas data on the phosphorylation status of β_2-AR at Ser346 and Ser(355,356) were normalized to total β_2-AR protein levels.

Statistical analysis. Values are expressed as the mean ± standard deviation (SD). SPSS 13 software (SPSS Inc., Chicago, IL, USA) was used to perform statistical analysis. All data were normally distributed. The unpaired Student's t-test was used

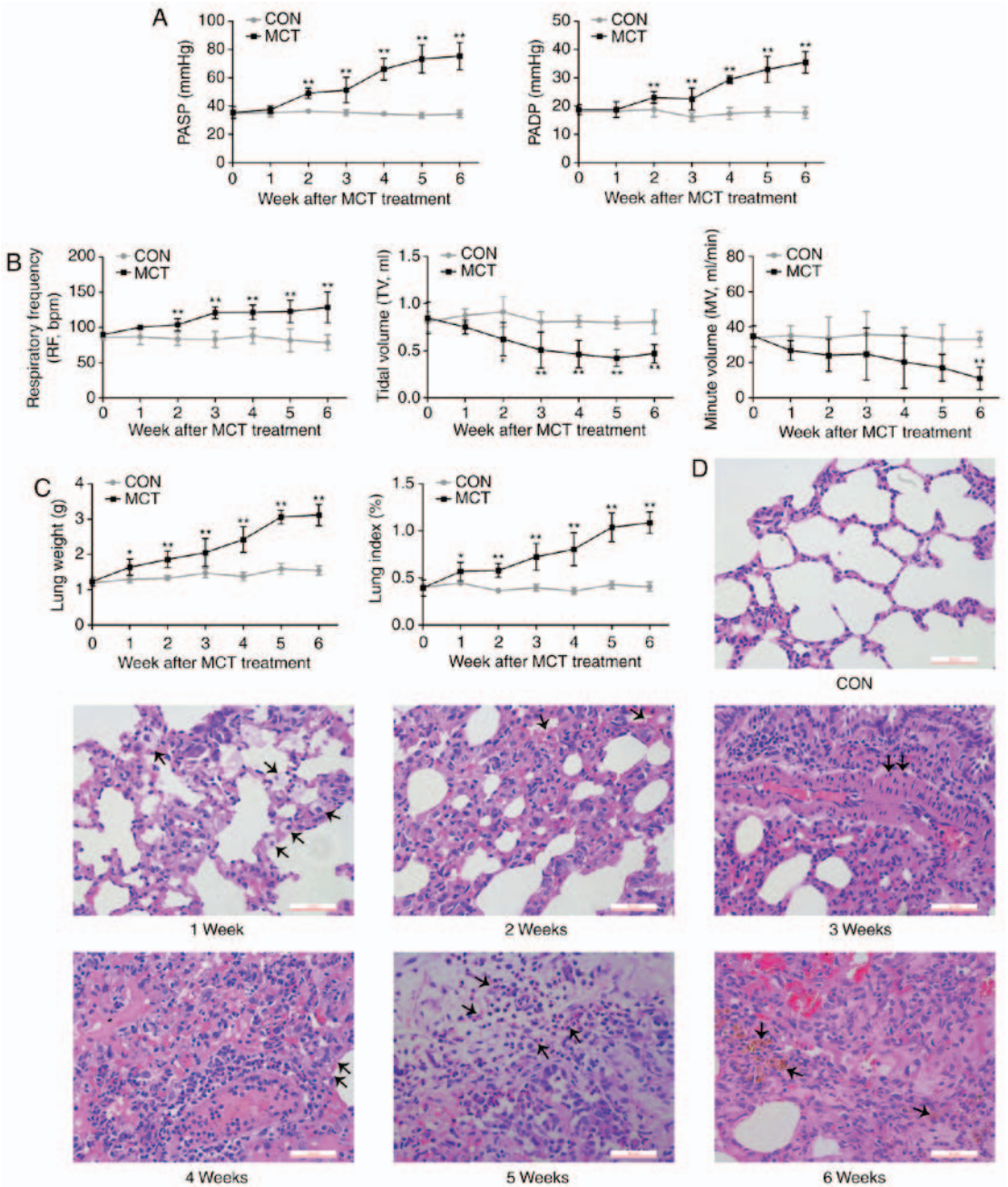

Figure 1. *In vivo* effects of MCT on lung function and structure. (A) PASP and PADP in the MCT group displayed a significant increase at weeks 2-6. (B) During disease progression, respiratory parameters, including respiratory frequency, TV and MV we recorded. A decreasing MV trend mirrored the significant decline in TV, while the RF remained significantly accelerated from week 2 to week 6 in MCT-treated rats compared with that in the control rats. (C and D) Histopathological changes in rats with MCT-induced pulmonary arterial hypertension were progressively aggravated from W1-6 (scale bar, 50 μm). W1, edema; W2, congestion; W3, thickening of arterial wall; W4, thickening of alveolar wall; W5, inflammatory cell infiltration; W6, pulmonary hemosiderosis (respective changes were indicated by arrows). Values are expressed as the mean ± standard deviation (n=10). *P<0.05 and **P<0.01 vs. the CON group. MCT, monocrotaline; CON, control; PASP, pulmonary artery systolic pressure; PADP, pulmonary arterial diastolic pressure; MV, minute volume; TV, tidal volume; RF, respiratory frequency; W, week.

to determine the significance between two groups. One-way analysis of variance was used for multiple comparisons, followed by post-hoc analysis [Dunett's test or least significant differences test]. P<0.05 was considered to indicate a statistically significant difference.

Results

Progressive deterioration of lung function and histopathology. PASP and PADP were increased from week 2 onwards (Fig. 1A). As an indication of respiratory dysfunction, the MV exhibited a declining trend from the early stages of PAH, becoming significantly lower compared with the baseline value at week 6, which was concurrent with a significantly increased RF and a reduced TV during PAH development (Fig. 1B). Concomitant with the results of pulmonary dysfunction, MCT-induced rats displayed an increasingly higher lung weight and lung index compared with that of CON-rats over the experimental period (Fig. 1C). The gradually aggravating histopathological changes of the lungs were characterized by interstitial edema,

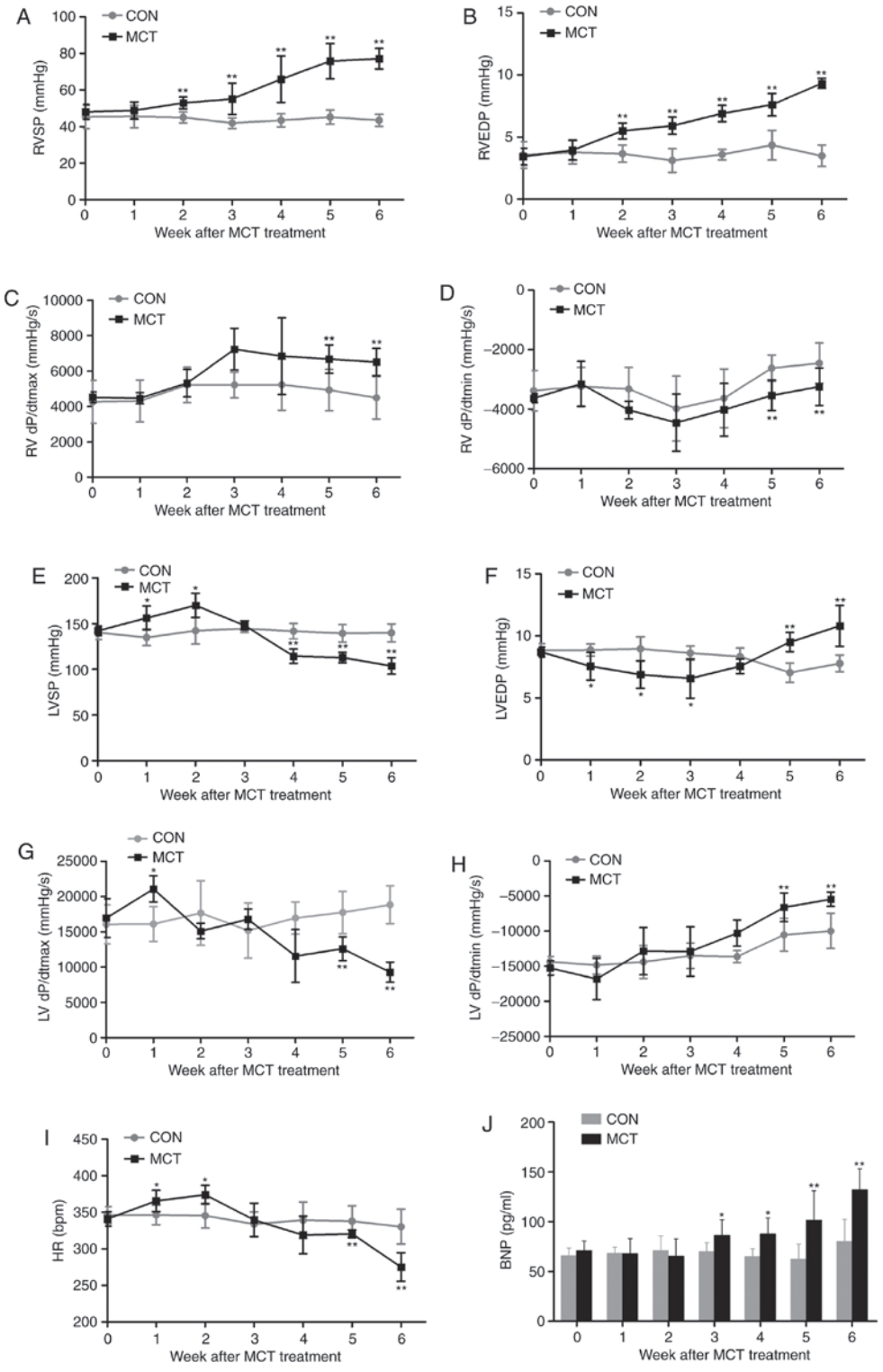

Figure 2. Hemodynamic characteristics of the heart and BNP augmentation during 6 weeks of MCT treatment. (A) The RVSP and (B) RVEDP significantly increased in rats with MCT-induced pulmonary arterial hypertension. (C and D) RV function was enhanced, as confirmed by the increase in the $+dP/dt_{max}$ and decrease in the $-dP/dt_{min}$. (E) The cardiac inotropic LVSP, (F) lusitropic LVEDP, (G) $+dP/dt_{max}$ in the LV, (H) $-dP/dt_{min}$ in the LV and (I) chronotropic HR in rats in the presence of MCT were evaluated by catheterization. (J) A significant increase in the level of plasma BNP due to the persistent pressure overload was revealed in MCT-treated rats. Values are expressed as the mean ± standard deviation (n=10). *P<0.05 and **P<0.01 vs. the CON group. MCT, monocrotaline; CON, control; RVSP/LVSP, right/left ventricular systolic pressure; RVEDP, right ventricular end-diastolic pressure; $+dP/dt_{max}$, maximal rate of ventricular pressure; $-dP/dt_{min}$, minimal rate of ventricular pressure; HR, heart rate; BNP, brain natriuretic peptide.

congestion, thickening of the alveolar septum, thickening of the tunica media of the pulmonary arteries, inflammatory cell infiltration into the thickened area and pulmonary hemosiderosis (Fig. 1D).

Dynamic changes of the heart hemodynamics. In MCT-induced rats, RVSP and RVEDP exhibited a continuous elevation from week 2 onwards, reaching relative increases of ~1.8- and ~2.7-fold, respectively, at week 6 (Fig. 2A and B). Of

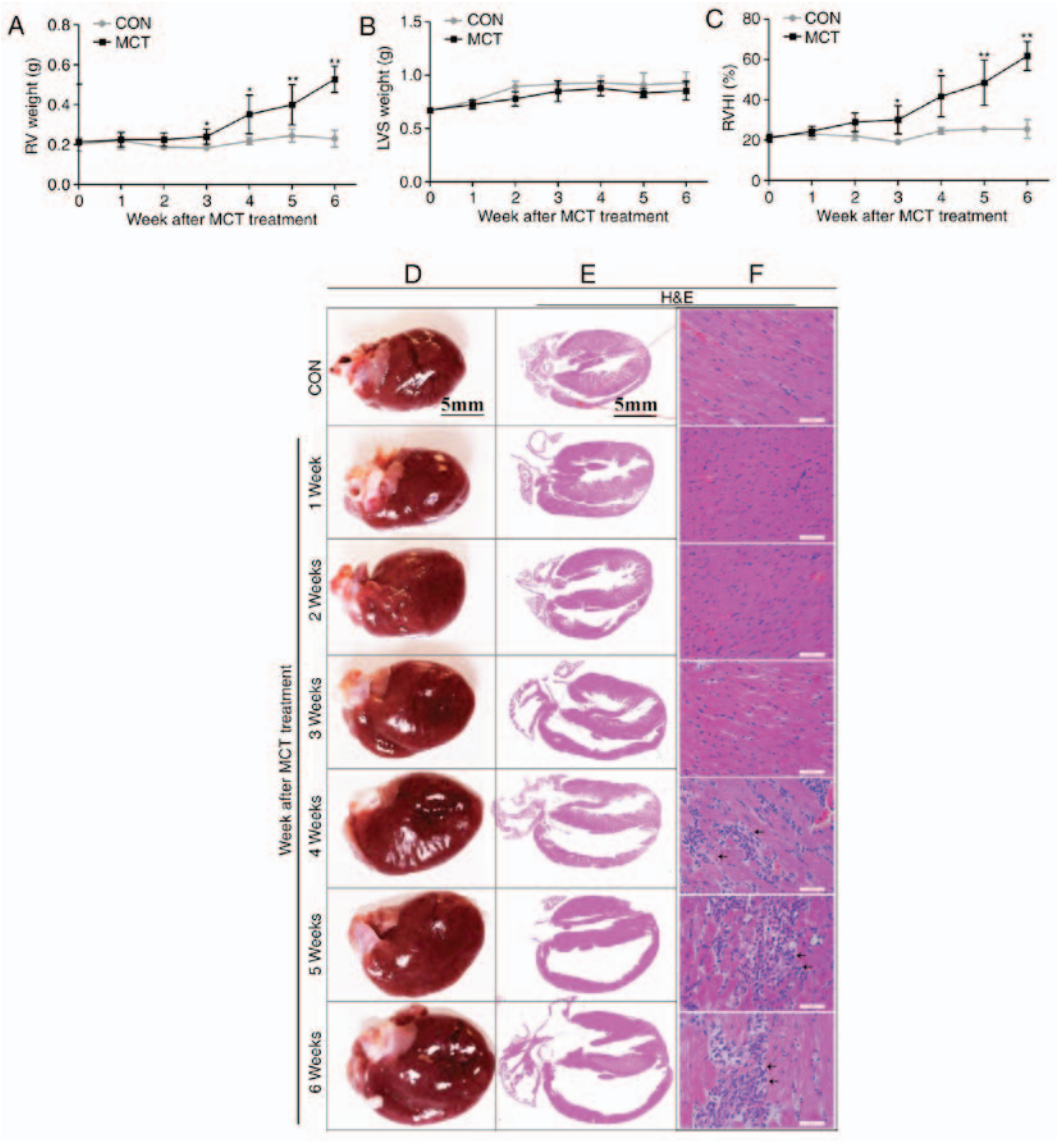

Figure 3. RV hypertrophy, dilatation and inflammation occurred concurrently during the development of pulmonary arterial hypertension. (A) The RV weight sharply increased at weeks 3-6. (B) The left ventricular weight, including the LVS, exhibited no significant change throughout the course of the experiment in MCT-induced rats. (C) The RVHI increased at weeks 3-6. (D) Gradually enlarged heart size and progressive dilatation of the right atrium and RV were observed on gross pathological examination (scale bar, 5 mm). (E and F) Histomorphometric analysis revealed a significant increase in diffuse inflammatory cell infiltration and widening of the interstitial space associated with progressive degeneration of cardiomyocytes from weeks 4-6 [indicated by arrows; scale bar, 5 mm in (E) and 50 μm in (F)]. Values are expressed as the mean ± standard deviation (n=10). *P<0.05 and **P<0.01 vs. the CON group. MCT, monocrotaline; CON, control; RV, right ventricular; RVHI, RV hypertrophy index; LVS, left ventricular and intraventricular septum.

note, improved RV contraction and relaxation were evidenced by $+dP/dt_{max}$ increasing from week 3 onwards and $-dP/dt_{min}$ significantly declining during weeks 5-6 (Fig. 2C and D). By contrast, LV function appeared to be initially compensated during weeks 1-2, as indicated by the elevated LVSP and $+dP/dt_{max}$, as well as the lowered LVEDP, and was eventually decompensated by weeks 5-6, as confirmed by a significantly decreased LVSP and $+dP/dt_{max}$, as well as an increased LVEDP and $-dP/dt_{min}$ (Fig. 2E-H). Similarly, the chronotropic curve of the HR was increased at weeks 1-2 and was significantly decreased by weeks 5-6 (Fig. 2I). In agreement with previous hemodynamic results, the ventricular response to persistent high pressure caused a time-dependent increase of the BNP in MCT-exposed rats by weeks 3-6, which was already notably increased by 65.39% at week 6 compared with the CON group (Fig. 2J).

Progressive maladaptive RV remodeling in the MCT-induced PAH model. The degree of RV hypertrophy was determined by the RV weight and the RVHI, and was identified to reach a significant level from week 3 onwards, whereas the LVS weight exhibited no significant change over time (Fig. 3A-C). In addition, on gross anatomical examination, RV dilatation was evident as a gradually progressive enlargement of the right atrial and RV volumes (Fig. 3D and E). These changes were accompanied by diffuse inflammatory cell infiltration and widening of the interstitial space from weeks 4-6, as assessed by H&E staining (Fig. 3F). In addition, as the disease progressed, the RV muscle exhibited typical characteristics of fibrosis, including the appearance of extensive interstitial and perivascular collagen deposition or fibrosis. Similar results were obtained by apoptosis detection using the TUNEL assay. As presented in Fig. 4, no marked myocardial fibrosis

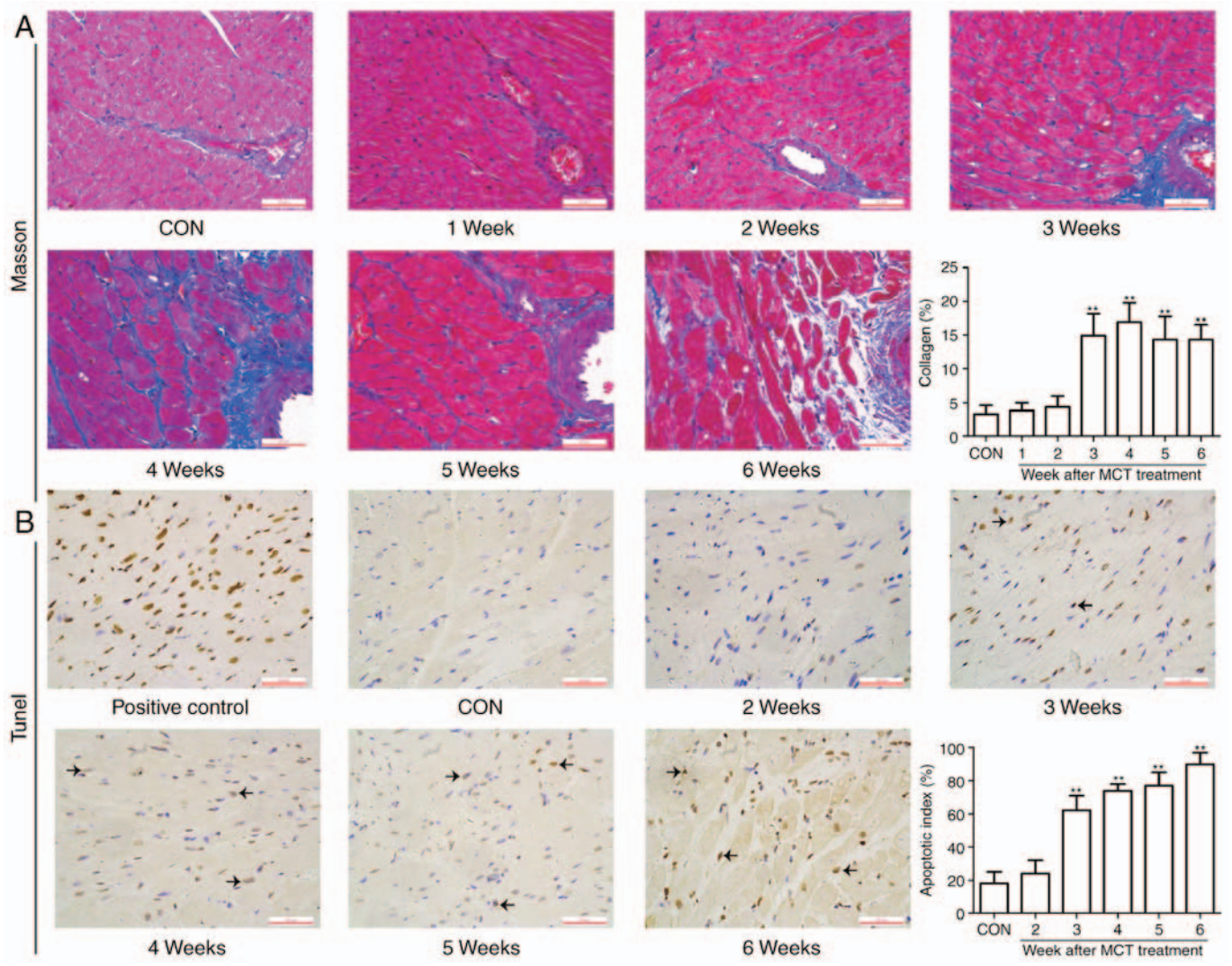

Figure 4. Myocardial fibrosis and apoptosis concur during RV remodeling by MCT-induced pressure overload. Representative images of (A) myocardial fibrosis examined by Masson's trichrome staining (collagen fibers were stained blue) and (B) myocardial cell apoptosis by TUNEL staining (TUNEL-positive cells were defined as cells with clear brown or brown-blue nuclear labeling; indicated by arrows) in the RV during the development of pulmonary arterial hypertension (scale bar, 50 μm). Quantitative analysis revealed that the extent of collagen deposition and the number of apoptotic cells were significantly increased at weeks 3-6 compared with those in the control group. Values are expressed as the mean ± standard deviation (n=5 slides per group). **P<0.01 vs. the CON group. MCT, monocrotaline; CON, control; RV, right ventricular; TUNEL, terminal deoxynucleotidyl transferase deoxyuridine triphosphate nick end labeling.

and apoptosis were observed at weeks 1-2, whereas they were significantly higher in the MCT group compared with those in the CON group from week 3 onwards. Taken together, these observations suggest that progressive maladaptive remodeling occurred in the RV during the MCT-induced development of PAH.

GPCR signaling contributes to RV remodeling. PCR array analysis demonstrated that pathological changes of RV remodeling were accompanied with an upregulation of genes associated with inflammation, hypertrophy, apoptosis and fibrosis, including interleukin (IL)1b, IL-1 receptor type 2 (IL1R2), endothelin 1 (EDN1), connective tissue growth factor (CTGF), matrix metalloproteinase 9 (MMP9) and serpin family E member 1 (Serpine1) (P<0.05; Fig. 5). In addition, in MCT-induced rats, angiotensin receptor (Agtr)-associated genes (Agt, Agtr1b and Agtr2) were upregulated at weeks 1-3 and then downregulated compared with the CON group by weeks 5 and/or 6 (Fig. 5). In addition, the expression of β_1-AR was downregulated by weeks 5-6 (Fig. 5).

β_2-AR signaling is involved in RV remodeling. To further investigate the molecular mechanisms of RV remodeling induced by PAH, the expression of β_1-AR and β_2-AR, as well as the phosphorylation of β_2-AR at two sites [pSer346 and pSer(355,356)] was measured, as was the expression of PKA, CaMKII and GRK2 (Fig. 6A). The results demonstrated that the expression of β_1-AR exhibited a slight increasing trend by weeks 2-3 and then rapidly declined by weeks 4-6 compared with the value at week 3. The expression of β_2-AR exhibited a slight decreasing trend over time (Fig. 6B). The PKA-dependent level of p-β_2-AR (Ser346) initially remained unchanged and then sharply increased by weeks 5-6, with a concomitant increase in the expression of PKA and CaMKII (Fig. 6C and D). However, the GRK-dependent level of p-β_2-AR [Ser(355,356)] was reduced by week

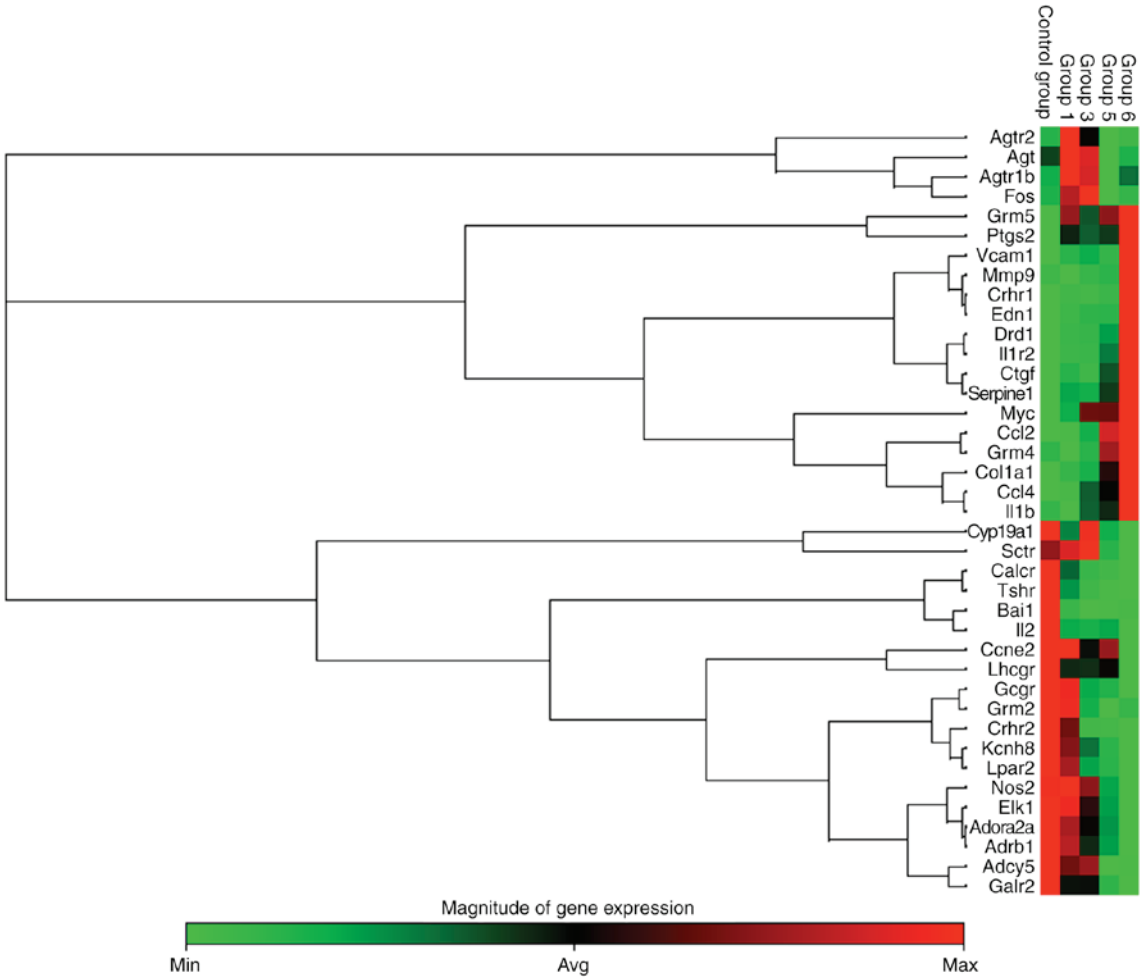

Figure 5. Heat map cluster representing 39 differentially expressed G protein-coupled receptor mRNAs from RV tissue determined by reverse transcription-quantitative polymerase chain reaction analysis. Differentially expressed mRNAs were selected among those that displayed fold changes of >2 or <0.5 compared with the control group (n=3 per group). Groups 1, 3, 5 and 6 correspond to the monocrotaline groups at weeks 1, 3, 5 and 6, respectively. Agtr2, angiotensin II receptor, type 2; Agt, angiotensinogen; Agtr1b, angiotensin II receptor, type 1b; Fos, fos proto-oncogene; Grm5, glutamate metabotropic receptor 5; Ptgs2, prostaglandin-endoperoxide synthase 2; Vcam1, vascular cell adhesion molecule 1; Mmp9, matrix metalloproteinase 9; Crhr1, corticotropin releasing hormone receptor1; EDN1, endothelin 1; Drd1, dopamine receptor D1; Il1r2, interleukin 1 receptor, type 2; Ctgf, connective tissue growth factor; Serpine1, serpin family E member 1; Myc, myc proto-oncogene; Ccl2, C-C motif chemokine ligand 2; Grm4, glutamate metabotropic receptor 4; Col1a1, collagen type I α1 chain; Ccl4, C-C motif chemokine ligand 4; Il1b, interleukin 1β; Cyp19a1, cytochrome P450, family 19, subfamily a, polypeptide 1; Sctr, secretin receptor; Calcr, calcitonin receptor; Tshr, thyroid stimulating hormone receptor; Bai1, brain-specific angiogenesis inhibitor 1; Il2, interleukin 2; Ccne2, Cyclin E2; Lhcgr, luteinizing hormone/choriogonadotropin receptor; Gcgr, glucagon receptor; Grm2, glutamate metabotropic receptor 2; Crhr2, corticotropin releasing hormone receptor 2; Kcnh8, potassium voltage-gated channel subfamily H member 8; Lpar2, lysophosphatidic acid receptor 2; Nos2, nitric oxide synthase 2; EIK-1, Ets-like transcription factor-1; Adora2a, adenosine A2a receptor; Adrb1, adrenoceptor β1; Adcy5, adenylate cyclase 5; Galr2, galanin receptor 2; RV, right ventricular; min, minimum; max, maximum; avg, average.

3 in comparison with that in the CON group, and was increased by weeks 5-6, while the levels of GRK2 remained unchanged (Fig. 6C and D).

Discussion

In the present study, the RV transitioned from initially adaptive remodeling caused by persistent PAH, to hyperfunction and maladaptive remodeling, as evidenced by hypertrophy, ventricular dilatation, inflammation, fibrosis and apoptosis, during the course of the disease. MCT injection initially resulted in functional and structural lung damage, which was accompanied by LV hyperfunction and subsequent adaptive hypertrophy of the RV. Consistently, in the early stages of PAH, the expression of the pSer(355,356) site of β_2-AR was significantly decreased in rats with MCT-induced PAH. As the disease progressed, concomitant with late maladaptive RV remodeling and apoptosis, upregulation of GPCR signaling and further β_2-AR-stimulatory G protein (G_s)-PKA/CaMKII signaling activation were observed in the late stages of PAH. The key finding of the present study was that the adaptive and maladaptive RV remodeling in the MCT-induced PAH model was accompanied by a distinct evolution in β_2-AR signaling, which may facilitate the treatment of progressive RV failure during PAH with appropriately timed drug intervention.

Following MCT treatment, structural damage and functional impairment were initially observed in the lungs, thereby producing irreversible PAH (increased PASP and PADP), further leading to RV hypertrophy and failure, which manifested with a marked elevation in RV weight and RVHI, hemodynamically by an increase in RVSP and RVEDP, and

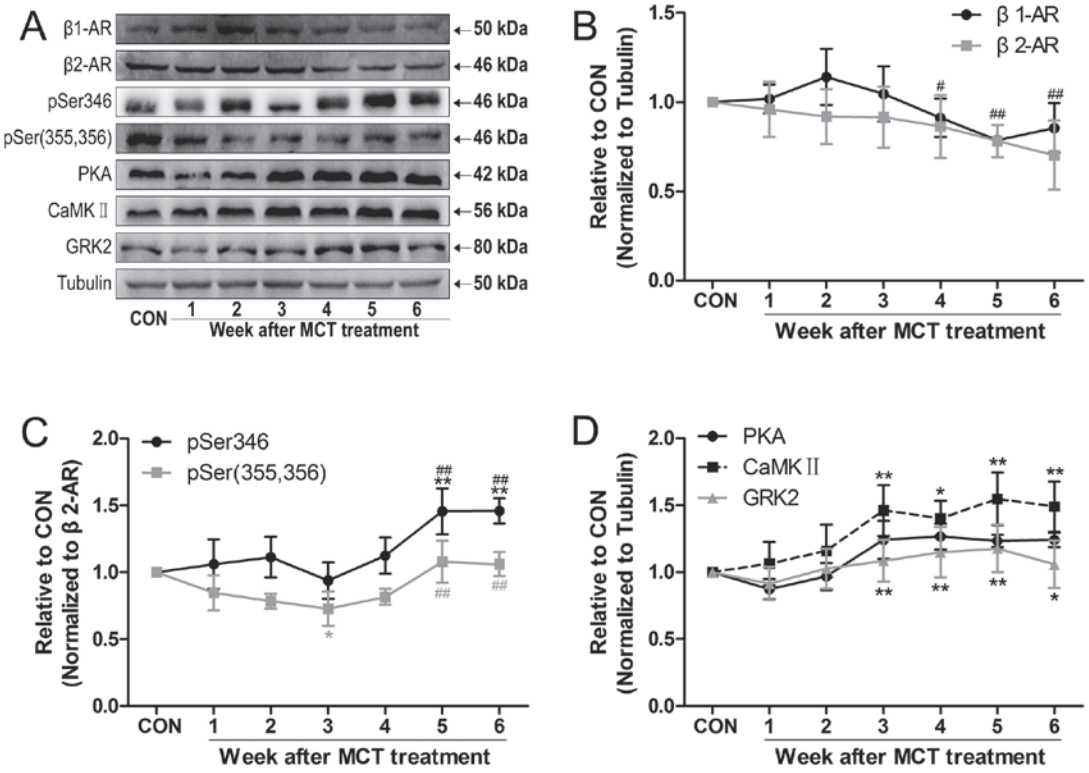

Figure 6. MCT treatment caused changes in the relative protein levels of β-AR in the RV free wall. (A) Representative western blot image of β-AR signaling-associated proteins in different groups. (B-D) Time-dependent changes in (B) β_1-AR and β_2-AR subtypes, (C) phosphorylation of the β_2-AR at the Ser346 and Ser(355,356) sites, and (D) PKA and CaMKII (a PKA-mediated downstream target of β-AR). A slight increasing trend was observed in the density of GRK2 expression. Values are expressed as the mean ± standard deviation (n=5 per group). *P<0.05 and **P<0.01 vs. the CON group; $^{\#}$P<0.05 and $^{\#\#}$P<0.01 vs. the week 3 group. MCT, monocrotaline; CON, control; RV, right ventricular; β-AR, β-adrenergic receptor; PKA, protein kinase A; CaMKII, Ca^{2+}/calmodulin-dependent kinase II; GRK2, G protein-coupled receptor kinase 2.

histopathologically by evidenced dilatation and inflammation. Of note, the present results, taken together with those of associated studies (11,34,35), revealed enhanced RV performance (increased $+dP/dt_{max}$ and decreased $-dP/dt_{min}$) in the late stages of PAH. However, despite this result, the RV pumping function was reduced (36), likely due to the markedly elevated afterload (increased PASP, PADP and RVSP) and preload (increased RVEDP). Hyperfunction leads to increased energy consumption and adverse cardiac remodeling in the failing heart. In the present study, Masson and TUNEL staining further confirmed the exacerbation of adverse RV remodeling, as evidenced by increased myocardial fibrosis and more apparent myocyte apoptosis. Mechanically, upregulation of GPCR-associated genes, including IL1b, IL1R2, EDN1, CTGF, MMP9 and Serpine1, were partly responsible for aggravated pathological alterations of the RV in the late stages of PAH. Assessment of the physiology revealed a noteworthy yet differential functional response of the heart to MCT. Although the RV systolic and diastolic performance increased following remodeling, the effects on the LV appeared to be different, with the initial increase being followed by reduced and compromised ventricular function (28). Overall, LV failure may be attributed to global neurohormonal adaptations, as defined by hyperactivity of the sympathetic nervous system (SNS) and the renin-angiotensin-aldosterone system (RAAS) (37,38). Hyperactivity of the SNS and RAAS were further demonstrated by upregulated angiotensin receptor-associated genes (Agt, Agtr1b and Agtr2) in the RV, and accelerated HR in the early stages of PAH. In advanced PAH, rats that were injected with MCT developed resistance to the sustained activation of SNS and RAAS, as validated by downregulated angiotensin receptor-associated genes and β_1-AR, as well as slow HR in the late stages of PAH. In addition, an elevation in BNP, which is considered a hallmark of HF (39,40), further confirmed the presence of overt HF. Taken together, these results support that the advancement of MCT-induced pulmonary inflammation and consolidation resulted in PAH, and further led to adverse RV remodeling and apoptosis and, eventually, overt HF.

A recent study suggested that nebivolol, a β_1-antagonist and $\beta_{2,3}$-agonist, induced partial relaxation of the pulmonary artery, altered PAH-associated endothelial dysfunction *in vitro* and improved experimental PAH in rats (26). In fact, the benefits of nebivolol in rats administered MCT may be restricted in the early stages (days 14-21) of PAH (7). Routinely, the prevalence of PAH increases as chronic obstructive pulmonary disease (COPD) worsens (5). β_2-agonists generally have bronchodilatory action and exert beneficial effects on pulmonary circulatory hemodynamics and RV performance in patients with COPD, hence delaying the occurrence and development of PAH. Furthermore, the present study documented that the GRK-dependent phosphorylation of β_2-AR at Ser(355,356) in the RV was significantly reduced, without changes in the PKA-dependent expression of pSer346 of β_2-AR in the early stages of PAH. In addition, it is known that β_2-AR activation by catecholamines has a key role in promoting the M2 regulatory macrophage (anti-inflammatory)

phenotype during endotoxemia and acute lung injury through the phosphoinositide 3-kinase pathway, but not the canonical cyclic adenosine monophosphate (cAMP)/PKA signaling pathway (41). Additionally, circulating monocyte/macrophage lineage cells contribute significantly to the pulmonary artery (PA) remodeling process in experimental PAH (42). On the basis of these findings, a preliminarily hypothesis may be that β_2-AR activation could promote the M2 regulatory macrophage phenotype to improve pulmonary vascular remodeling in PAH. Thus, there is a rationale for a potential benefit of β_2-agonist therapy in this stage.

As the disease progressed, however, cardiotoxic effects develop with respect to β_2-AR activation in the failing heart (17-22,43,44). Under normal physiological conditions, the predominant β_1-AR subtype is the major mediator of cardiac contractility. However, under pathological conditions (failing heart, advanced age), the β_1-AR response to sustained high circulating catecholamine levels may result in β_1-AR downregulation and mediate myocyte apoptosis through PKA-dependent or PKA-independent CaMKII activation (1,14,15,37). By contrast, the contribution of the more minor β_2-AR subtype to cardiac contractility is more prominent (45). This is an important hypothesis, as β_2-AR activation may be associated with enhanced RV contractility mediated by G_s-biased β_2-AR (increased phosphorylation of the pSer346 site)/PKA signaling activation in the late stages of PAH. Moreover, G_s-biased β_2-AR activation may also change to a cell-wide cyclic adenosine monophosphate (cAMP) signal propagation pattern and acquire the characteristics of the β_1-AR response in the failing heart, as evidenced by PKA-dependent stimulation of CaMKII signaling in the present study, thus promoting the HF phenotype (22).

In support of this result, compelling evidence has demonstrated that β-blockade treatment prevented pathological RV remodeling and improved RV function in MCT-induced PAH models (25,27,28). Furthermore, several clinical studies have reported the beneficial effect of β-blockade therapy on PAH-RVF (46-48). In addition, β-blockade also improved LV function (28,38,49). Finally, a series of studies by our group have demonstrated that the combination of the traditional Chinese medicines Fuzi (*Aconiti Lateralis* radix praeparata, which may activate β_2-AR) and Beimu (*Fritillariae Thunbergii* bulbus) significantly improved lung function and reduced pulmonary histopathological changes in the early stages of PAH (29,50). However, as the disease progressed, the combination of Fuzi and Beimu increased the risk of developing severe cardiac adverse effects by synergistically activating the cAMP-PKA-CaMKII signaling pathway in the late stages of the same PAH model. These results suggest that the enhanced RV contractility and concomitant activation of β_2-AR signaling occur in the late stages of PAH, which subsequently accelerates the adverse RV remodeling and apoptosis during the progression of PAH.

Of note, the present study had certain limitations. First, since β_1-AR and β_2-AR are associated with cardiotoxic effects and acceleration of HF, further study is required to demonstrate the causality of whether changes in β_1-AR or β_2-AR signaling may be associated with RV remodeling and apoptosis during the progression of PAH, e.g. by using β-AR inhibitors in the same model or β-AR agonists in similar experiments. The results of the present study indicated changes in the expression of PKA, GRK2 and β-ARs proteins, which may provide a novel theoretical approach according to which β-ARs are the key factors leading to RV remodeling induced by PAH. However, this role remains to be determined by gain- and loss-of-function strategies (including overexpression and silencing of these genes) in further studies. In addition, it is required to further investigate whether the variability in the expression of GRKs, including GRK-5 and -6, has any significance in MCT-treated rat hearts. Furthermore it should be examined whether the dynamic changes observed in RV are associated with concomitant changes in the LV. Finally, the significance of inflammatory cells in the pulmonary artery remodeling process is currently attracting increasing attention (42). It is also known that macrophage activation and β_2-AR have an important role in inflammation (41). The hypoxic rat model is particularly useful in the evaluation of anti-inflammatory therapies, since circulating monocytic cell populations significantly contributing to the pulmonary artery remodeling process is a key feature in this PAH model (42). However, the present study mainly focuses on the association of β_2-AR with the progression of RV remodeling. Further investigation is required to confirm the role of β_2-AR through the anti-inflammatory M2 regulatory macrophage phenotype in PA remodeling, particularly in an animal model of hypoxic PAH.

In conclusion, the present study observed initial lung injury following MCT injection, which was accompanied by unchanged PKA-mediated phosphorylation of β_2-AR and decreased GRK-mediated phosphorylation of β_2-AR in the early stages of PAH. As the disease progressed, a marked increase in maladaptive RV remodeling and concomitant cardiomyocyte apoptosis were observed in the late stages of PAH, which was accompanied by GPCR signaling alterations and β_2-AR-G_s-PKA/CaMKII signaling activation. Having established that the development of PAH in rats is characterized by distinct evolutionary β_2-AR signaling changes, this knowledge must be applied in the clinical setting by appropriately timed administration of either β_2-agonists or non-selective β-AR blockade therapy, to avoid the development of PAH.

Acknowledgements

The present study was supported by the National Natural Science Foundation of China (grant no. 81773920), the National Basic Research Program of China (973 program; grant nos. 2011CB505300 and 2011CB505302) and the Program for Changjiang Scholars and Innovative Research Team in University (grant no. IRT_14R41).

Competing interests

The authors declare that they have no competing interests.

References

1. Ryan JJ, Huston J, Kutty S, Hatton ND, Bowman L, Tian L, Herr JE, Johri AM and Archer SL: Right ventricular adaptation and failure in pulmonary arterial hypertension. Can J Cardiol 31: 391-406, 2015.

2. Vonk-Noordegraaf A, Haddad F, Chin KM, Forfia PR, Kawut SM, Lumens J, Naeije R, Newman J, Oudiz RJ, Provencher S, *et al*: Right heart adaptation to pulmonary arterial hypertension: Physiology and pathobiology. J Am Coll Cardiol 62: (Suppl 25): D22-D33, 2013.
3. Hardziyenka M, Campian ME, Reesink HJ, Surie S, Bouma BJ, Groenink M, Klemens CA, Beekman L, Remme CA, Bresser P and Tan HL: Right ventricular failure following chronic pressure overload is associated with reduction in left ventricular mass: Evidence for atrophic remodeling. J Am Coll Cardiol 57: 921-928, 2011.
4. Hsia HH and Haddad F: Pulmonary hypertension: A stage for ventricular interdependence? J Am Coll Cardiol 59: 2203-2205, 2012.
5. Lee-Chiong Jr TL and Matthay RA: Pulmonary hypertension and cor pulmonale in COPD. Semin Respir Crit Care Med 24: 263-272, 2003.
6. Montani D, Gunther S, Dorfmuller P, Perros F, Girerd B, Garcia G, Jaïs X, Savale L, Artaud-Macari E, Price LC, *et al*: Pulmonary arterial hypertension. Orphanet J Rare Dis 8: 97, 2013.
7. Rubin LJ: The beta-adrenergic receptor in pulmonary arterial hypertension: A novel therapeutic target? J Am Coll Cardiol 65: 681-683, 2015.
8. Mendes-Ferreira P, Santos-Ribeiro D, Adão R, Maia-Rocha C, Mendes-Ferreira M, Sousa-Mendes C, Leite-Moreira AF and Brás-Silva C: Distinct right ventricle remodeling in response to pressure overload in the rat. Am J Physiol Hear Circ Physiol 311: H85-H95, 2016.
9. Rain S, Handoko ML, Trip P, Gan CT, Westerhof N, Stienen GJ, Paulus WJ, Ottenheijm CA, Marcus JT, Dorfmüller P, *et al*: Right ventricular diastolic impairment in patients with pulmonary arterial hypertension. Circulation 128: 2025-2025, 2013.
10. Campian ME, Verberne HJ, Hardziyenka M, de Bruin K, Selwaness M, van den Hoff MJ, Ruijter JM, van Eck-Smit BL, de Bakker JM and Tan HL: Serial noninvasive assessment of apoptosis during right ventricular disease progression in rats. J Nucl Med 50: 1371-1377, 2009.
11. Paffett ML, Hesterman J, Candelaria G, Lucas S, Anderson T, Irwin D, Hoppin J, Norenberg J and Campen MJ: Longitudinal in vivo SPECT/CT imaging reveals morphological changes and cardiopulmonary apoptosis in a rodent model of pulmonary arterial hypertension. PLoS One 7: e40910, 2012.
12. Wang Y, Ouyang M, Wang Q and Jian Z: MicroRNA-142-3p inhibits hypoxia/reoxygenation-induced apoptosis and fibrosis of cardiomyocytes by targeting high mobility group box 1. Int J Mol Med 38: 1377-1386, 2016.
13. Bisognano JD, Weinberger HD, Bohlmeyer TJ, Pende A, Raynolds MV, Sastravaha A, Roden R, Asano K, Blaxall BC, Wu SC, *et al*: Myocardial-directed overexpression of the human beta(1)-adrenergic receptor in transgenic mice. J Mol Cell Cardiol 32: 817-830, 2000.
14. Iwai-Kanai E, Hasegawa K, Araki M, Kakita T, Morimoto T and Sasayama S: alpha- and beta-adrenergic pathways differentially regulate cell type-specific apoptosis in rat cardiac myocytes. Circulation 100: 305-311, 1999.
15. Zhang X, Szeto C, Gao E, Tang M, Jin J, Fu Q, Makarewich C, Ai X, Li Y, Tang A, *et al*: Cardiotoxic and cardioprotective features of chronic β-adrenergic signaling. Circ Res 112: 498-509, 2013.
16. Lymperopoulos A, Rengo G and Koch WJ: Adrenergic nervous system in heart failure: Pathophysiology and therapy. Circ Res 113: 739-753, 2013.
17. Woo AY, Song Y, Xiao RP and Zhu W: Biased β2-adrenoceptor signalling in heart failure: Pathophysiology and drug discovery. Br J Pharmacol 172: 5444-5456, 2015.
18. Daaka Y, Luttrell LM and Lefkowitz RJ: Switching of the coupling of the beta2-adrenergic receptor to different G proteins by protein kinase A. Nature 390: 88-91, 1997.
19. Rengo G, Lymperopoulos A, Leosco D and Koch WJ: GRK2 as a novel gene therapy target in heart failure. J Mol Cell Cardiol 50: 785-792, 2011.
20. Salazar NC, Vallejos X, Siryk A, Rengo G, Cannavo A, Liccardo D, De Lucia C, Gao E, Leosco D, Koch WJ and Lymperopoulos A: GRK2 blockade with βARKct is essential for cardiac β2-adrenergic receptor signaling towards increased contractility. Cell Commun Signal 11: 64, 2013.
21. Zhu W, Petrashevskaya N, Ren S, Zhao A, Chakir K, Gao E, Chuprun JK, Wang Y, Talan M, Dorn GW II, *et al*: Gi-biased β2AR signaling links GRK2 upregulation to heart failure. Circ Res 110: 265-274, 2012.
22. Nikolaev VO, Moshkov A, Lyon AR, Miragoli M, Novak P, Paur H, Lohse MJ, Korchev YE, Harding SE and Gorelik J: Beta2-adrenergic receptor redistribution in heart failure changes cAMP compartmentation. Science 327: 1653-1657, 2010.
23. Lang D, Holzem K, Kang C, Xiao M, Hwang HJ, Ewald GA, Yamada KA and Efimov IR: Arrhythmogenic remodeling of β2 versus β1 adrenergic signaling in the human failing heart. Circ Arrhythmia Electrophysiol 8: 409-419, 2015.
24. Wang Y, Yuan J, Qian Z, Zhang X, Chen Y, Hou X and Zou J: β2 adrenergic receptor activation governs cardiac repolarization and arrhythmogenesis in a guinea pig model of heart failure. Sci Rep 5: 7681, 2015.
25. Bogaard HJ, Natarajan R, Mizuno S, Abbate A, Chang PJ, Chau VQ, Hoke NN, Kraskauskas D, Kasper M, Salloum FN and Voelkel NF: Adrenergic receptor blockade reverses right heart remodeling and dysfunction in pulmonary hypertensive rats. Am J Respir Crit Care Med 182: 652-660, 2010.
26. Perros F, Ranchoux B, Izikki M, Bentebbal S, Happé C, Antigny F, Jourdon P, Dorfmüller P, Lecerf F, Fadel E, *et al*: Nebivolol for improving endothelial dysfunction, pulmonary vascular remodeling, and right heart function in pulmonary hypertension. J Am Coll Cardiol 65: 668-680, 2015.
27. Ishikawa M, Sato N, Asai K, Takano T and Mizuno K: Effects of a pure alpha/beta-adrenergic receptor blocker on monocrotaline-induced pulmonary arterial hypertension with right ventricular hypertrophy in rats. Circ J 73: 2337-2341, 2009.
28. Okumura K, Kato H, Honjo O, Breitling S, Kuebler WM, Sun M and Friedberg MK: Carvedilol improves biventricular fibrosis and function in experimental pulmonary hypertension. J Mol Med 93: 663-674, 2015.
29. Zhuang P, Huang Y, Lu Z, Yang Z, Xu L, Sun F, Zhang Y and Duan J: cAMP-PKA-CaMKII signaling pathway is involved in aggravated cardiotoxicity during fuzi and beimu combination treatment of experimental pulmonary hypertension. Sci Rep 6: 34903, 2016.
30. Deten A, Millar H and Zimmer HG: Catheterization of pulmonary artery in rats with an ultraminiature catheter pressure transducer. Am J Physiol Circ Physiol 285: H2212-H2217, 2003.
31. Schmittgen TD, Lee EJ, Jiang J, Sarkar A, Yang L, Elton TS and Chen C: Real-time PCR quantification of precursor and mature microRNA. Methods 44: 31-38, 2008.
32. Chen C, Ridzon DA, Broomer AJ, Zhou Z, Lee DH, Nguyen JT, Barbisin M, Xu NL, Mahuvakar VR, Andersen MR, *et al*: Real-time quantification of microRNAs by stem-loop RT-PCR. Nucleic Acids Res 33: e179, 2005.
33. Zhuang P, Zhang Y, Cui G, Bian Y, Zhang M, Zhang J, Liu Y, Yang X, Isaiah AO, Lin Y and Jiang Y: Direct stimulation of adult neural stem/progenitor cells in vitro and neurogenesis in vivo by salvianolic acid B. PLoS One 7: e35636, 2012.
34. Hessel MH, Steendijk P, den Adel B, Schutte CI and van der Laarse A: Characterization of right ventricular function after monocrotaline-induced pulmonary hypertension in the intact rat. Am J Physiol Hear Circ Physiol 291: H2424-H2430, 2006.
35. Werchan PM, Summer WR, Gerdes AM and McDonough KH: Right ventricular performance after monocrotaline-induced pulmonary hypertension. Am J Physiol Circ Physiol 256: H1328-H1336, 1989.
36. Kuehne T, Yilmaz S, Steendijk P, Moore P, Groenink M, Saaed M, Weber O, Higgins CB, Ewert P, Fleck E, *et al*: Magnetic resonance imaging analysis of right ventricular pressure-volume loops in vivo validation and clinical application in patients with pulmonary hypertension. Circulation 110: 2010-2016, 2004.
37. Ameri P, Bertero E, Meliota G, Cheli M, Canepa M, Brunelli C and Balbi M: Neurohormonal activation and pharmacological inhibition in pulmonary arterial hypertension and related right ventricular failure. Hear Fail Rev 21: 539-547, 2016.
38. Usui S, Yao A, Hatano M, Kohmoto O, Takahashi T, Nagai R and Kinugawa K: Upregulated neurohumoral factors are associated with left ventricular remodeling and poor prognosis in rats with monocrotaline-induced pulmonary arterial hypertension. Circ J 70: 1208-1215, 2006.
39. Giannakoulas G, Mouratoglou SA, Gatzoulis MA and Karvounis H: Blood biomarkers and their potential role in pulmonary arterial hypertension associated with congenital heart disease. A systematic review. Int J Cardiol 174: 618-623, 2014.
40. Luchner A, Hengstenberg C, Löwel H, Riegger GA, Schunkert H and Holmer S: Effect of compensated renal dysfunction on approved heart failure markers direct comparison of brain natriuretic peptide (BNP) and N-terminal pro-BNP. Hypertension 46: 118-123, 2005.

41. Grailer JJ, Haggadone MD, Sarma JV, Zetoune FS and Ward PA: Induction of M2 regulatory macrophages through the β2-adrenergic receptor with protection during endotoxemia and acute lung injury. J Innate Immun 6: 607-618, 2014.
42. Burke DL, Frid MG, Kunrath CL, Karoor V, Anwar A, Wagner BD, Strassheim D and Stenmark KR: Sustained hypoxia promotes the development of a pulmonary artery-specific chronic inflammatory microenvironment. Am J Physiol Lung Cell Mol Physiol 297: L238-L250, 2009.
43. Baker AJ: Adrenergic signaling in heart failure: A balance of toxic and protective effects. Pflugers Arch 466: 1139-1150, 2014.
44. Fajardo G, Zhao M, Urashima T, Farahani S, Hu DQ, Reddy S and Bernstein D: Deletion of the β2-adrenergic receptor prevents the development of cardiomyopathy in mice. J Mol Cell Cardiol 63: 155-164, 2013.
45. Rybin VO, Pak E, Alcott S and Steinberg SF: Developmental changes in beta2-adrenergic receptor signaling in ventricular myocytes: The role of Gi proteins and caveolae microdomains. Mol Pharmacol 63: 1338-1348, 2003.
46. So PP, Davies RA, Chandy G, Stewart D, Beanlands RS, Haddad H, Pugliese C and Mielniczuk LM: Usefulness of beta-blocker therapy and outcomes in patients with pulmonary arterial hypertension. Am J Cardiol 109: 1504-1509, 2012.
47. Thenappan T, Roy SS, Duval S, Glassner-Kolmin C and Gomberg-Maitland M: β-blocker therapy is not associated with adverse outcomes in patients with pulmonary arterial hypertension: A propensity score analysis. Circ Hear Fail 7: 903-910, 2014.
48. Bandyopadhyay D, Bajaj NS, Zein J, Minai OA and Dweik RA: Outcomes of β-blocker use in pulmonary arterial hypertension: A propensity-matched analysis. Eur Respir J 46: 750-760, 2015.
49. Chatterjee S, Udell JA, Sardar P, Lichstein E and Ryan JJ: Comparable benefit of β-blocker therapy in heart failure across regions of the world: Meta-analysis of randomized clinical trials. Can J Cardiol 30: 898-903, 2014.
50. Yang Z, Lu ZQ, Zhang YJ, Li YB, Wang ZY, Zhang YL, Zhuang PW and Bai G: Looking for agonists of β2 adrenergic receptor from Fuzi and Chuanwu by virtual screening and dual-luciferase reporter assay. J Asian Nat Prod Res 18: 550-561, 2016.